3D-Fractography in Bending-Torsion Fatigue

Štěpán Major[1], Petr Ponížil[2], Karel Slámečka[1] and Jaroslav Pokluda[1]

[1] Institute of Engineering Physics, Brno University of Technology, Technická 2, 616 69 Brno, Czech Republic, s.major@seznam.cz, pokluda@ufi.fme.vutbr.cz.
[2] Department of Physics and Materials Engineering, Tomas Bata University in Zlin, sq. TGM 588, 762 72 Zlin, Czech Republic.

ABSTRACT. *A stereophotogrammetrical analysis in SEM is used to investigate the fracture morphology of the high-strength low-alloy steel generated under combined bending-torsion fatigue loading. Changes in many roughness parameters are presented for two series of profiles parallel and perpendicular to the local crack propagation direction in dependence on both the fatigue life and the loading ratio* $r= \tau_a /(\tau_a+ \sigma_a)$ *(*σ_a *is the bending amplitude and* τ_a *is the torsion amplitude). Profile's fractal parameters are also calculated as "scale-independent" characteristics. Statistical distributions of facet angles with respect to the horizontal plane revealed prevailing orientations of local crack growth directions in various mixed-mode loading cases. One of the interesting results is that many roughness parameters start to increase rapidly above a critical value of loading ratio* $r_c \approx 0.5$.

INTRODUCTION

Quantitative fractography has been used as a tool in materials research since the fracture surface can be considered to be a measure of the degradation process [1-7]. The surface roughness is usually extremely enhanced when a high portion of lower to medium amplitudes of shear loading modes II and III is applied [3]. In such cases the crack usually propagates in extremely complicated manner making local arrests and forming a branch/twist morphology or so-called factory roofs [1-4]. In the contrary a high amount of opening loading mode or, sometimes, a high-amplitude of shear loading lead to a macroscopically flat surface.

The efforts to approach fractography in a more quantitative way has led to many interesting studies on the interconnection between the surface morphology and loading (or environmental) conditions [5-16]. However, the most crucial problem in the quantitative fractography remains to be a significant lack of experimental data from fracture surfaces created by biaxial loading [9]. This paper deals with several types of roughness parameters characterising the morphology variation produced by a combined bending-torsion loading.

EXPERIMENTAL PROCEDURE

Fatigue Experiments

Fatigue experiments were performed using the resonance testing machine MZGS-100. Five smooth specimens of high-strength low-alloy steel (yield stress R_e = 805 MPa and ultimate stress R_m = 930MPa) were loaded until a final failure. Bending and torsion loadings (frequency 29 Hz, R = -1) and their synchronous in-phase combinations were applied at room temperature. Loading settings and achieved fatigue life data are collected in Tab. 1, where σ_a is the bending amplitude, τ_a is the torsion amplitude, r is the loading ratio, $r = \tau_a /(\tau_a + \sigma_a)$, and N_f is the number of cycles to failure. The fatigue life N_f of investigated specimens was in the order of 10^6 cycles (high cycle fatigue).

Table 1. Experimental data

Type of loading	σ_a [MPa]	τ_a [MPa]	r [-]	N_f
Pure bending	620	0	0	1229000
Combined bending-torsion	550	200	0.23	1252000
Combined bending-torsion	330	330	0.5	1099100
Combined bending-torsion	140	385	0.73	1700150
Pure torsion	0	390	1	4475000

Stereophotogrammetrical Reconstruction of Fracture Surface

Stereogrammetry is based on the software evaluation of two digitalized images of fracture surface taken from different positions of view [15]. Stereoimages of selected parts of fracture surface on each specimen were acquired using the scanning electron microscope Leo S440 and the tilting angle of stereopairs was 10º. The commercial software MeX was used for data processing. The output of the procedure is the digital elevation model of the depicted surface region consisting of up to 30.000 nonequidistantly localised points.

Profile and Fractal Parameters

In order to evaluate different aspect of roughness, several types of parameters were adapted. Profile amplitude parameters depending only on changes in vertical z-coordinate are represented by the vertical profile range R_z, which is simply given as a difference between the highest and the lowest points of the profile, and the arithmetic roughness R_a, also known as a centre line average. The arithmetic roughness is defined as

$$R_a = \frac{1}{N}\sum_{i=1}^{N}\left|z_i - z_M\right|, \tag{1}$$

where N is a number of valid data points and z_M is the mean height value. Hybrid parameters affected by both the amplitude and the spacing of asperities are represented by the linear roughness R_L [11]. It is defined as a ratio of the true profile length L and its projected length L_P:

$$R_L = \frac{L}{L_P} \quad . \tag{2}$$

The other hybrid parameter is the vertical roughness R_V:

$$R_V = \frac{h}{L_P}, \tag{3}$$

where h is the sum of height differences between adjacent profile points.

A self-similarity of fracture morphology can be quantified by its fractal dimension D. Since different experimental techniques lead to different estimated values of fractal dimensions for real, quasi-similar, fracture profiles [17-19], two different fractal methods were taken into account. The box counting method is based on the following equation:

$$N(\eta) \propto \eta^{-D_B}, \tag{4}$$

where D_B is the box counting fractal dimension. The plane in which a curve is plotted is divided into squares of the side length η, and the number of squares N intersecting the curve is counted. The second algorithm was based on the divider method. The measured length dependece on the measurement unit η can be expressed as

$$L(\eta) \propto \eta^{-(D_D-1)}, \tag{5}$$

where D_D is the divider fractal dimension.

Analysed Profiles

For each specimen the square area of size 0.16 mm^2 was chosen with its centre at the distance of 0.76 mm from the crack initiation site located on the specimen surface. Using Delaunay triangulation [20-21], two sets of 50 profiles were traced for all analysed areas. In order to evaluate different position of the progressing macrocrack front, the first set laid in the crack propagation direction and the second one perpendicular to this direction.

RESULTS AND DISCUSION

In all presented Figures, curves for particular specimen are labelled by values of the loading ratio r. Parameter R_z calculated for profiles parallel and perpendicular to the crack propagation direction is plotted in Fig. 1. Significantly higher values R_z in both directions correspond to specimens with the loading ratio higher then 0.5. Results for R_a in Fig. 2 show similar behaviour. Values of both the vertical range and the arithmetic roughness are somewhat higher for profiles taken in the direction parallel to the crack growth. Results for the linear roughness R_L and the vertical roughness R_V are shown in

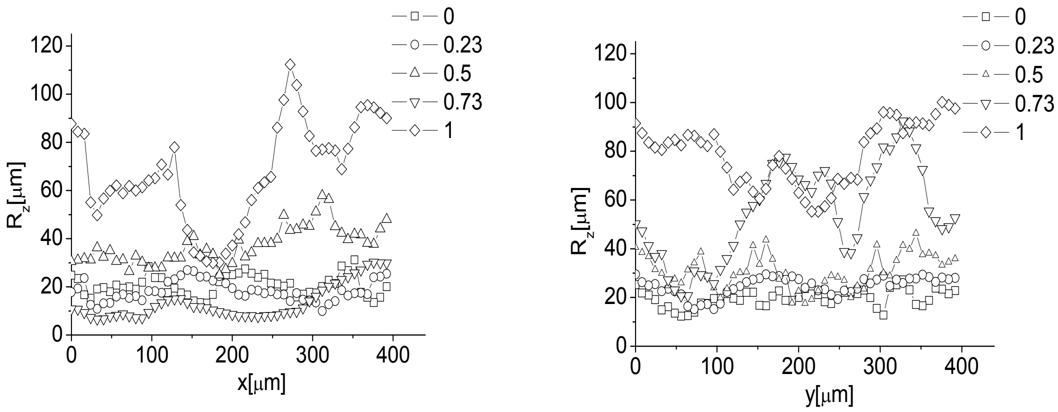

Figure 1. The vertical range R_z of profiles parallel (x-axis) and perpendicular (y-axis) to the local crack propagation direction.

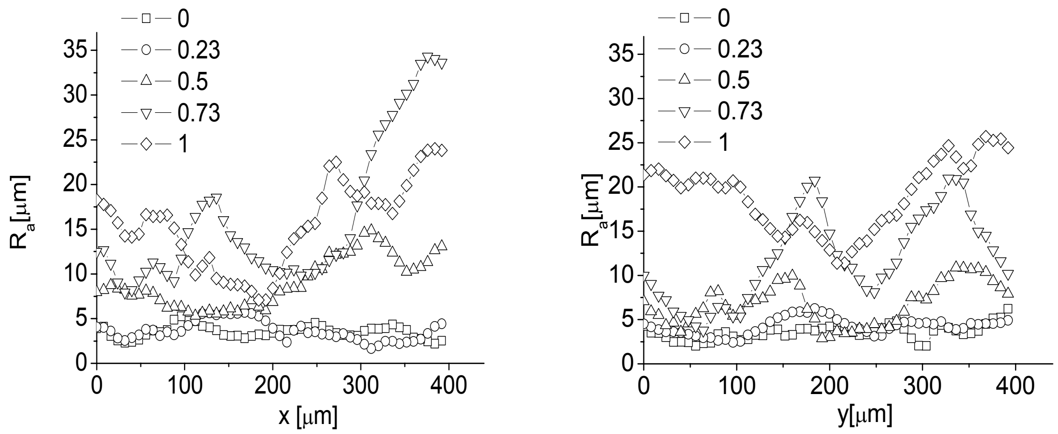

Figure 2. The arithmetic roughness R_a of profiles parallel (x-axis) and perpendicular (y-axis) to the local crack propagation direction.

Figs. 3 and 4. For both directions, again, the highest values are achieved for the pure torsion and the lowest R_L and R_V are detected for the pure bending. The dependence of the mean values of R_L and R_a on the ratio r in the direction parallel to the local crack propagation is plotted in Fig. 5. A steep increase of both parameters starts closely before reaching the value $r = 0.5$, in agreement with results reported for the low-cycle fatigue region [22]. Figs. 6 and 7 show fractal dimensions D_D and D_B. There is no significant

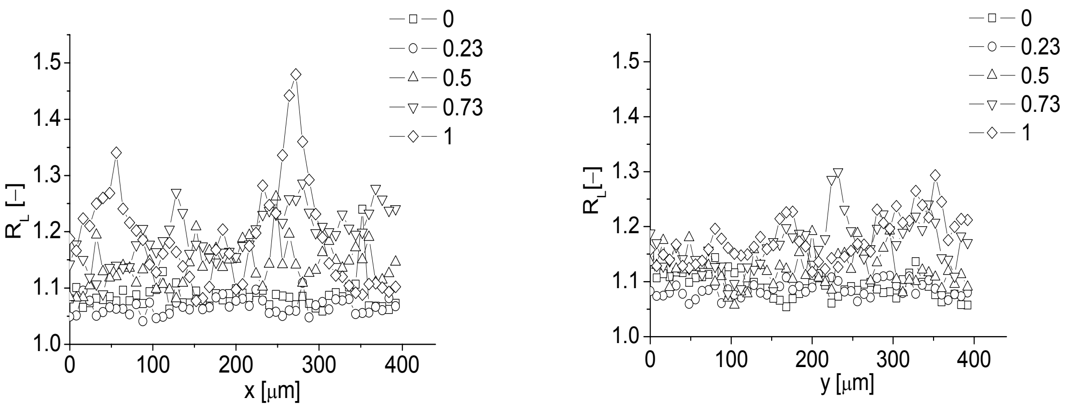

Figure 3. The linear roughness R_L of profiles parallel (x-axis) and perpendicular (y-axis) to the local crack propagation direction.

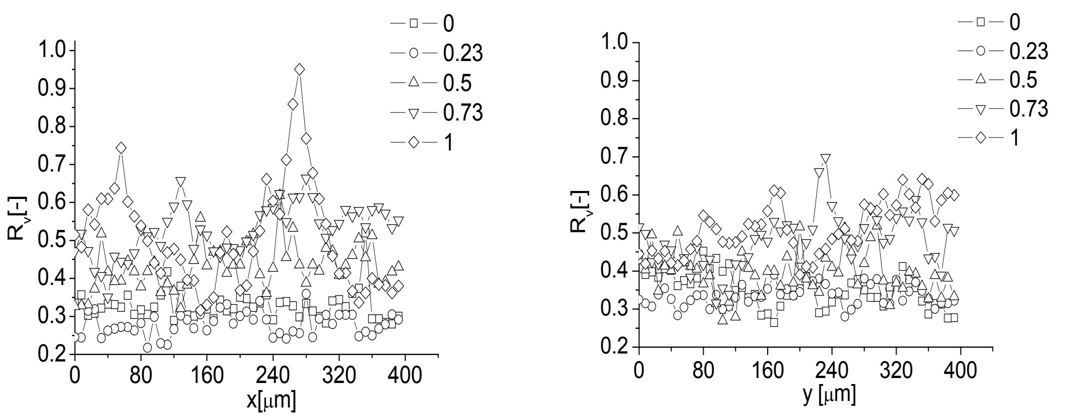

Figure 4. The vertical roughness R_V of profiles parallel (x-axis) and perpendicular (y-axis) to the local crack propagation direction.

relation between r and D_D or D_B . Values of both fractal dimensions strongly differ, D_B is changing in the range of 0.96-1.18 and D_D in the range of 1.03-1.08. Therefore, the method used for determination of the fractal dimension seems to be very important and should be always presented.

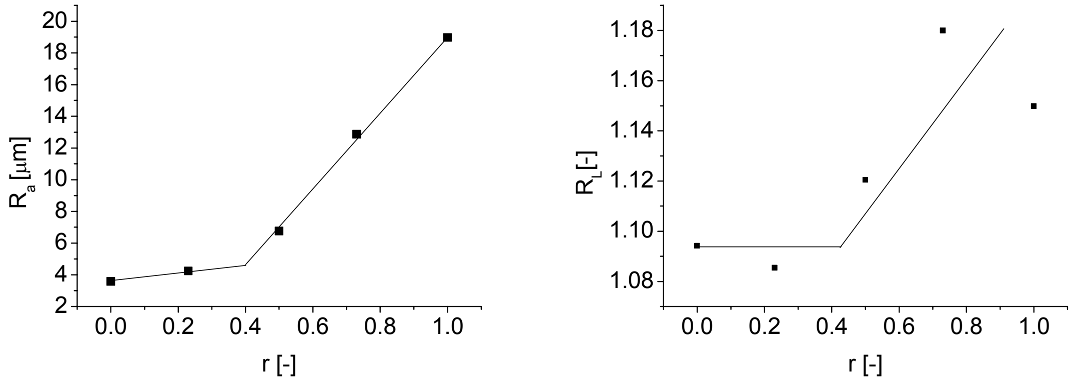

Figure 5. The dependence of roughness parameters on the loading ratio.

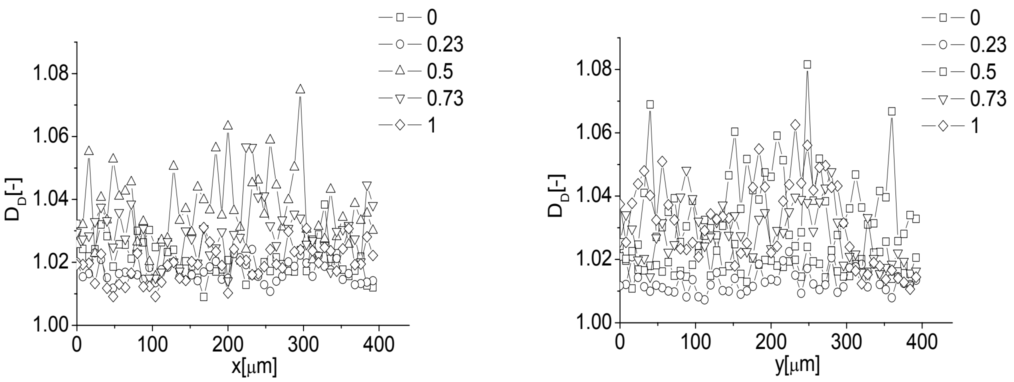

Figure 6. The fractal dimension D_D of parallel and perpendicular profiles.

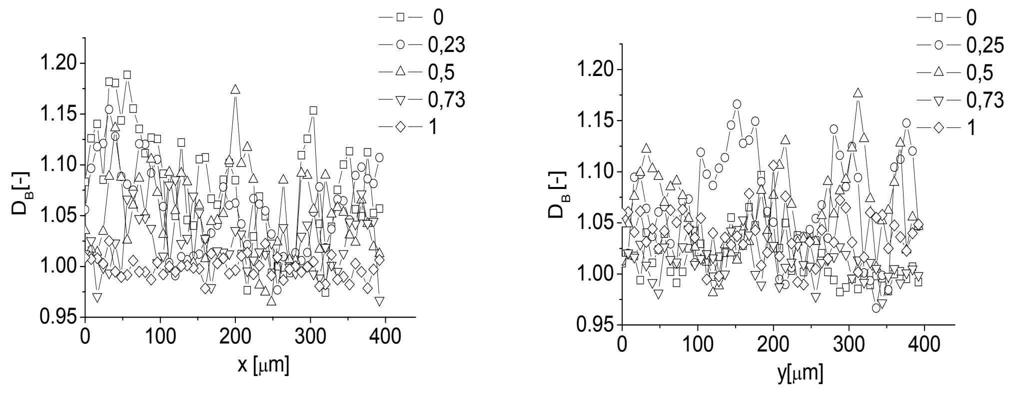

Figure 7. The fractal dimension D_B of parallel and perpendicular profiles.

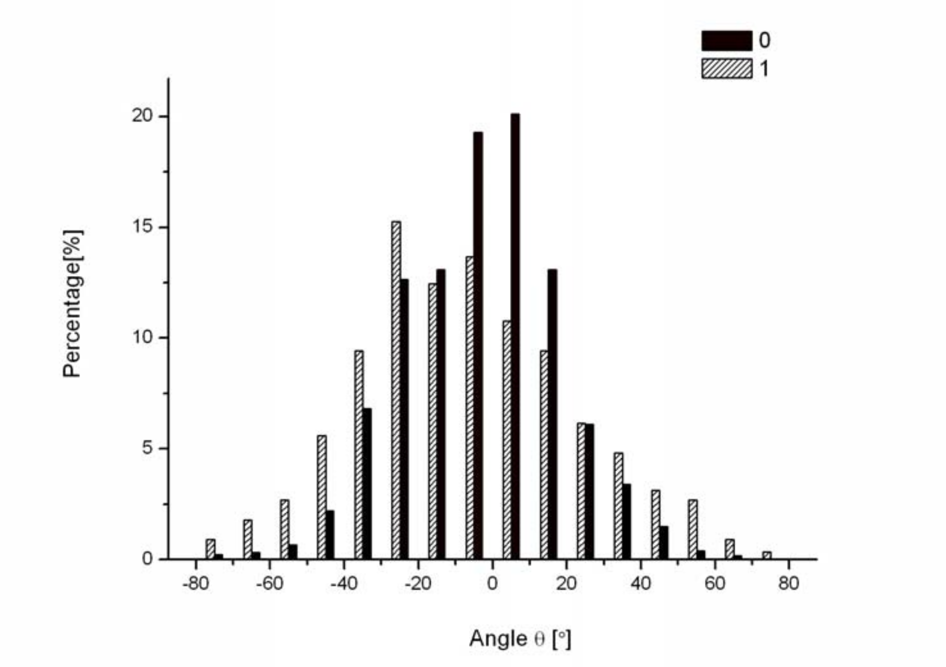

Figure 8. The angular distribution of facets for loading ratios $r = 0$ (pure bending) and $r = 1$ (pure torsion).

The histograms of the angular distribution for pure bending and pure torsion are shown in Fig. 8. In case of torsion, the angles higher then 40° (or lower then - 40°) occur more frequently than in case of bending. On the contrary, the low angles within the range of -20° to 20° are preferred on the fracture surfaces produced by bending.

CONCLUSION

The most important results can be summarized in the following points:

(i) Roughness parameters R_z, R_a, R_L, R_v significantly increase above a critical value $r_c \approx 0.5$ (the torsion loading component is equal to the bending one).

(ii) In case of pure torsion angles higher then 40° (or lower then - 40°) occur more frequently than in case of pure bending. The contrary holds for the low angles within the range of -20° to 20°.

(iii) There is no significant relationship between fractal dimensions D_D and D_B and the ratio of loading components.

ACKNOWLEDGEMENT

Authors acknowledge the support of the Ministry of Education of the Czech Republic and the Czech Science Foundation in the frame of the respective research plan MSM 0021630518 (J. Pokluda) and the project No GA106/05/0550 (P. Ponížil).

REFERENCES

1. Vaziri, A., Nayeb-Hashemi (2005) *Engng. Fract. Mechanics* **72**, 617-629.
2. Socie, D.F., Marquis, G.B. (2000) *Multiaxial Fatigue*, Society of Automotive Engineers Inc., Warrendale.
3. Pokluda, J., Pippan, R. (2005) *Fatigue Fract. Engng. Mater. Struct. Mater.* **28**, 179-185.
4. Pook, L.P. (2002) *Crack Paths*, Wit Press.
5. Antunes, F.V., Ramalho, A., Ferreira, J.M. (2000) *Int. J. Fatigue.* **22**, 781-788.
6. Kojabayashi, T., Shockey, D.A. (2001) *Int. J. Fatigue.* **23,** S135-S142.
7. Li, X.W., Tian, J.F., Han, N.L., Kang, Z., Wang, Z.G. (1996) *Mater. Letters* **29,** 235-240.
8. Lauschmann, H., Nedbal, I., (2002) *Image Anal. Stereol.* **21,** 139-144.
9. Slámečka, K., Pokluda, J. (2004) in: *Advenced Fracture Mechanics for Life and Safety Assesments* (ECF15), KTH, Stockholm, CD.
10. Dooley, P., Bernasek, S.L. (1998) *Surf. Sience* **406**, 206-220.
11. Underwood, E.E., Banerjee, K. (1992) in: *Metals Handbook Vol.12,* ASM International, Metals Park, Ohio, USA, 193-210.
12. Underwood, E.E., Banerjee, K. (1992) in: *Metals Handbook Vol.12,* ASM International, Metals Park, Ohio, USA, 212-215.
13. Gadelmawla, E.S., Koura, M.M., Maksoud, T.M.A., Elewa, I.M., Soliman, H.H. (2002) *J. Mat. Proc. Technol*. **123**, 133-145.
14. Slámečka, K., Pokluda, J. (2005) *Mater. Sci. Forum* **482,** 263-266.
15. Scher, S., Kolednik, O. (2001) *Europ. Microsc. Analysis*, **March 2001**, 15-17.
16. Lockwood, W.D., Reynolds, A.P., (1999) *Mater. Characterization* **42**, 123-134.
17. Charluk, E., Bigerelle, M., Iost, A., (1998) *Engng. Fract. Mech.* **61,** 119-139.
18. Balankin, A.S. (1997) *Engng. Fract. Mechanics* **57,** 135-203.
19. Naito, K., Fujii, T. (1995) *Int. J. Adhesion and Adhesives* **15**,123-130.
20. Okabe, A., Boots, B., Sugihara, K., Chin,S-N. (2000) *Spatial Tessellations: Concepts and Applications of Voronoi Diagrams*, 2nd edition, John Wiley, Chichester.
21. Ponížil, P. (1999) *Voronoi tessellations generated by Point cluster field,. PhD Thesis,* Faculty of Technology Zlín, Czech Republic.
22. Slámečka, K., Pokluda, J. (2005) *Mater. Sci. & Eng. A* (in print).